

Three-dimensional time-resolved optical mammography of the uncompressed breast

Louise C. Enfield,^{1,*} Adam P. Gibson,¹ Nicholas L. Everdell,¹ David T. Delpy,¹ Martin Schweiger,² Simon R. Arridge,² Caroline Richardson,³ Mohammad Keshtgar,³ Michael Douek,³ and Jeremy C. Hebden¹

¹Department of Medical Physics and Bioengineering, University College London, Gower Street, London, WC1E 6BT, UK

²Department of Computer Science, University College London, Gower Street, London, WC1E 6BT, UK

³Department of Surgery, University College London, 4th Floor, The Medical School Building, 74 Huntley Street, London, WC1E 6AU, UK

*Corresponding author: lenfield@medphys.ucl.ac.uk

Received 30 October 2006; revised 24 January 2007; accepted 31 January 2007;
posted 31 January 2007 (Doc. ID 76581); published 18 May 2007

Optical tomography is being developed as a means of detecting and specifying disease in the adult female breast. We present a series of clinical three-dimensional optical images obtained with a 32-channel time-resolved system and a liquid-coupled interface. Patients place their breasts in a hemispherical cup to which sources and detectors are coupled, and the remaining space is filled with a highly scattering fluid. A cohort of 38 patients has been scanned, with a variety of benign and malignant lesions. Images show that hypervascularization associated with tumors provides very high contrast due to increased absorption by hemoglobin. Only half of the fibroadenomas scanned could be observed, but of those that could be detected, all but one revealed an apparent increase in blood volume and a decrease in scatter and oxygen saturation. © 2007 Optical Society of America

OCIS codes: 110.6960, 170.3830.

1. Introduction

Breast cancer is responsible for nearly one third of cancer cases and one fifth of cancer deaths in women in the UK, which represents ~40,000 cases and ~12,000 deaths each year [1]. Early detection decreases mortality [2], so many countries in the developed world routinely screen for breast cancer. The most commonly used breast-imaging tool is x-ray mammography [3]. However, x-ray mammography has a number of disadvantages: specificity is poor for some types of tumor, which can lead to unnecessary biopsies; it uses potentially hazardous ionizing radiation; and some women report that the required compression of the breast is painful. Mammography is also less suitable for younger women due to the increased density of the breast tissue. In cases involving younger women, ultrasound or magnetic resonance imaging

(MRI) is used [4,5], although neither of these techniques is suitable for screening asymptomatic women. Therefore a safe and effective imaging technique that can provide a distinction between benign and malignant lesions would be of very considerable benefit.

The use of near-infrared (NIR) light to examine the breast has been actively researched since the 1980s, when developments in source, detector, and computing technology made diffuse optical imaging feasible. So-called optical mammography provides discrimination between tissues based on their optical properties obtained from measurements of transmitted light [6–8]. In principle, the different spectral absorption characteristics of deoxyhemoglobin and oxyhemoglobin allow images to be derived from blood volume and blood oxygen saturation [9,10]. This provides valuable physiological information, which can also be used, if necessary, combined with anatomical imaging methods such as x-ray mammography or ultrasound [11]. Many research groups have built and begun to clinically evaluate optical imaging systems,

0003-6935/07/173628-11\$15.00/0

© 2007 Optical Society of America

based on a variety of measurement types (e.g., continuous intensity, time and frequency domain) at various NIR wavelengths [12–19]. One of the major challenges of optical mammography is to adequately couple a large number of optical sources and detectors to the breast, and various methods have been explored. Some groups use a compressed breast geometry [14,16,17], where one or more sources and detectors are scanned over both surfaces, and a single projection image is produced. A disadvantage of this method is that compression can lead to discomfort, especially in women suffering from sore breasts. An alternative method is to use a fixed array of source and detectors that surround the breast, from which either two-dimensional (2D) slices or a whole volume image can be reconstructed [12,18,19].

Over the past two or three years, there has been a large number of clinical studies published by various research groups. A research group at Physikalische-Technische Bundesanstalt, Berlin, has conducted a major study of the *in vivo* blood concentration and oxygen saturation in breast tumors, using a dual-wavelength time-domain optical mammography system [16,20,21]. Using a triple wavelength scanning (compression geometry) time-resolved imaging system, craniocaudal and mediolateral projections were recorded from 154 patients suspected of having breast cancer [20,21]. Images representing absorption, scatter, total hemoglobin concentration, and blood oxygen saturation were derived for each patient. Out of 102 histologically confirmed tumors, 72 were detected in both views, 20 in just one projection, and 10 were not detectable at all [20]. On average, tumor absorption coefficients were 2.5 times greater than surrounding tissue at 670 nm, and reduced scattering coefficients of tumors were 20% higher than surrounding tissue at 670 nm. Hemoglobin concentrations were systematically larger in tumors than in surrounding tissue, although blood oxygen saturation was found to be a poor discriminator between healthy and tumor tissue [21].

Meanwhile, researchers at the Politecnico di Milano have developed a similar scanning time-resolved optical mammography system, which has been used to scan 194 patients [17,22,23]. In the first part of their study, 101 patients with 114 lesions were scanned with a four-wavelength system. To improve the spectral content of the images, the system was expanded to seven wavelengths (637–985 nm). Images revealed sensitivity to tissue composition (oxy- and deoxyhemoglobin, water, lipids) and physiology (blood volume and oxygenation), as well as structural changes. An 80% detection rate for cysts and malignant lesion types was found when images were acquired in both craniocaudal and oblique views. Cancers exhibited an increased absorption coefficient compared with surrounding tissue, while cysts had a lower reduced scattering coefficient. The detection rate for other benign lesions such as fibroadenomas was much lower (<40%).

A breast-imaging system developed at Dartmouth College is based on 16 sources and 16 detectors

mounted on linear translation stages arranged in three circular arrays [24]. The patient lies prone with her breast suspended within the arrays, and the sources and/or detectors are moved in direct contact. Variations in hemoglobin, water content, and tissue-scattering properties between subjects have been observed, and changes over the menstrual cycle have been explored [19]. The parameters vary greatly between subjects, indicating that tumor hemoglobin concentration relative to background rather than absolute values may be a better diagnostic indicator. Studies have shown that tumors have a higher hemoglobin concentration and higher oxygen saturation compared with background [25] and that images representing the scattering properties often highlight lesions relative to surrounding healthy tissue [26].

A research group at the University of Pennsylvania has developed and tested a combined frequency domain and continuous-wave clinical system that employs six wavelengths [14]. The prone subject's breast is lightly compressed in an Intralipid-filled tank, and sources and detectors are placed on either side. Intralipid is a fat emulsion that is widely used for optical tissue equivalent phantoms. The system has also been combined with positron emission tomography (PET) using labeled fluorodeoxyglucose (FDG) to examine metabolic activity [27] and with MRI to provide simultaneous anatomical and physiological data [28]. A case study of a patient undergoing neoadjuvant chemotherapy with MRI and optical imaging showed a decrease in tumor size, in agreement with MRI [28]. A decrease in the total hemoglobin concentration contrast between the tumor and healthy tissue was also observed. The group has also been looking at the use of extrinsic contrast agents such as indocyanine green (ICG) to examine the uptake and outflow of the dye in tumors and healthy breast tissue [29].

A breast-imaging system has been developed by a team at the State University of New York that allows both breasts to be imaged simultaneously [12]. The system employs four wavelengths (between 760 and 830 nm) and 32 source–detector fibers for each breast. The subject lies with her breast pendant in the imaging array, and the optical fibers are translated radially until they are in direct contact with the breast. Data have been collected from a healthy volunteer and from a patient with a 6 cm ductal carcinoma in her left breast. Both were recorded at rest and when performing a controlled Valsalva maneuver. Data showed a marked difference between the data in the dynamic response of the cancerous versus the healthy breast [12].

The combination of optical imaging with conventional diagnostic modalities is also being investigated by researchers at Massachusetts General Hospital. Optical imaging probes have been integrated into an x-ray mammography system by mounting detectors and sources on removable compression plates [30]. Optical and x-ray data are recorded successively with the breast held in the same position. Scans on 18 patients with benign and malignant lesions revealed an increase in optical absorption near the benign and

malignant lesions, as well as in the dense fibroglandular tissue, relative to the surrounding tissues.

The *in vivo* optical properties of breast lesions and healthy tissues have also been extensively investigated by a group at the University of California, Irvine, who have developed a hand-held optical probe, which is placed against the breast. Diffuse reflection measurements are made at points on the surface of the breast [31]. Studies on 12 premenopausal patients with cancer show significant contrast between normal and tumor regions in the concentrations of deoxyhemoglobin, oxyhemoglobin, water, and lipids [31].

The contribution of our group at University College London (UCL) toward the development of optical mammography is based upon a 32-channel time-resolved optical imaging system [32]. Our initial measurements on patients were performed using a simple interface consisting of two rings of different sizes, to which the sources and detectors were attached, mounted on a frame [18]. The breast was placed into whichever ring provided the better fit for that patient. Twenty-one patients were scanned, with 17 out of 19 lesions being detected, including one subject scanned repeatedly over one year [18,33]. However, certain limitations were identified, such as inconsistent coupling between the fibers and the breast. This led to unusable intensity data and subsequently to an inability to distinguish between the scatter and absorption properties of the tissue. The fixed rings also proved unsuitable for older women as the breast tissue was too pendulous. Furthermore, a lesion may be missed if it was not located within or near the plane of the ring. To overcome these problems, an alternative patient interface has been developed [34], based on an approach originally adopted by Philips Research Laboratories [7]. The patient lies with her breast in a hemispherical cup filled with tissue-like intralipid-based scattering fluid. This method had three major benefits. First, cups can be made of a sufficient size to accommodate a large range of breast sizes and shapes, enabling the entire three-dimensional (3D) volume of the breast to be sampled. Second, the coupling of the source–detector optics at the surface is constant and independent of the subject, enabling intensity to be used as a data type in the image reconstruction. And third, the external geometry of the reconstructed volume is known exactly, so an accurate model can be generated. Initial experiments using isolated absorbing and scattering targets within the cup were conducted to evaluate the performance of the system in terms of the contrast, spatial resolution, and localization accuracy [34]. Results indicated that these parameters were strongly dependent on the location of the targets within the imaged volume. Initial studies on several healthy volunteers revealed subtle heterogeneity, particularity in the distribution of scatter. In this paper, we summarize the results of subsequent scans performed on a cohort of 38 patients with a range of benign and malignant lesions.

2. Methods

A. University College London Optical Tomography System

The UCL 32-channel time-resolved optical imaging system [32] employs a portable fiber laser (IMRA Inc., USA) that produces pulses ~ 2 ps in duration at 780 and 815 nm, interlaced with a repetition rate of 80 MHz. The pulses are transmitted through a 32-way optical switch that illuminates each source fiber in sequence. Each source fiber is integrated along the axis of a detector fiber bundle. The bundles transmit light to four eight-anode microchannel-plate photomultiplier tubes (MCP-PMTs). The MCP-PMTs produce an electronic pulse for each photon detected and are protected from overexposure by variable optical attenuators. Timing electronics record the times taken for photons to travel through the illuminated medium and produce a time-of-flight histogram known as a temporal point-spread function (TPSF) for each source–detector combination. Images are reconstructed (Subsection 2.D) using data types extracted from the TPSFs, such as integrated intensity, mean flight time, and variance. For the studies reported here, intensity and mean flight time have been used, as they have been proven to be most robust and the most effective at separating scatter and absorption [18].

B. Liquid-Coupled Interface

To accommodate breasts of different sizes, three rigid hemispherical cups were constructed, with diameters of 130, 160, and 180 mm, and depths of 70, 85, and 100 mm. Each was made by coating a latex rubber hemisphere with a 5 mm thickness of fiberglass impregnated with polyester resin (KS55, Alec Tiranti Ltd., London, UK) mixed with black polyester paint (Alec Tiranti Ltd., London, UK). Thirty-one regularly spaced 1 cm diameter holes were made in the hemisphere surface and Perspex windows were fixed into each hole, providing a watertight volume [34]. The optical fiber bundles are attached to the exterior surface of the cup by inserting them within short plastic tubes fixed over each window. Despite having made three different cups, the 160 mm diameter cup has proven to be sufficient for the vast majority of patients, and all the results presented here were obtained using this cup. The cup is attached to a plastic ring that fits within an aperture in a wooden table, as shown in Fig. 1. The coupling fluid that fills the remaining space between the breast and the hemisphere is made from a solution of Intralipid and near-infrared dye in de-ionized water, which provides an absorption coefficient of $\mu_a = 0.004 \text{ mm}^{-1}$ and a transport scatter coefficient of $\mu_s' = 0.8 \text{ mm}^{-1}$ at 800 nm. These values were chosen to ensure that the signal acquired for the largest source–detector separation produces a measured photon count rate of ~ 50 – 100 photons/s, sufficient to obtain useful data types for image reconstruction. The cup is filled with fluid from below using a peristaltic pump, which then

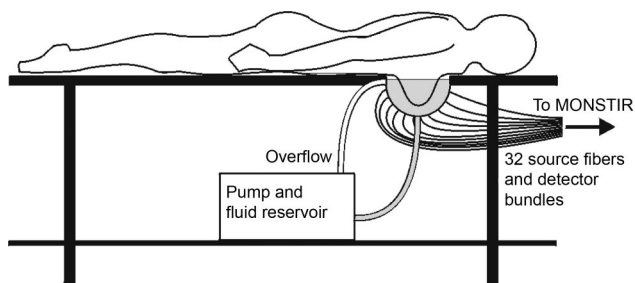


Fig. 1. Fluid-coupled patient interface for the 3D optical breast imaging. The patient lies with her breast pendant in a hemispherical cup filled with scattering fluid.

circulates fluid continuously and slowly to maintain a constant level of fluid. A channel is cut into the ring, which allows coupling fluid that overflows from the cup to return via plastic tubing to the fluid reservoir, where it is maintained at a constant temperature of 37 °C using an electrically isolated water heater. The table is covered with a layer of foam, and a pillow and towels are provided. Patients lie prone with either breast pendant in the cup, and most have reported no discomfort within scan times of between 5 and 20 min. The fluid-filled cup mounted in the table is shown in Fig. 2.

As reported previously [34], imaging using the hemispherical cup employs a so-called difference approach, which involves reconstructing the changes in optical properties between the cup containing both the coupling fluid and the breast and those of the cup containing the fluid alone. This eliminates the effect of uncertainty and variability in the surface coupling, allowing use of intensity measurements. The disadvantage of difference imaging is that errors will occur if the properties of the reference medium are not known exactly. To provide an adequate reference for patient studies it is necessary to extend the height of the reference medium beyond the top surface of the fluid-filled cup, since light traveling between sources and detectors located near the top of the cup can migrate into and out of the chest wall. This extension was provided using a thin, hollow latex cylinder, of height 100 mm and diameter 200 mm, mechanically supported by a plastic ring. To acquire a reference measurement the cylinder is placed on top of the

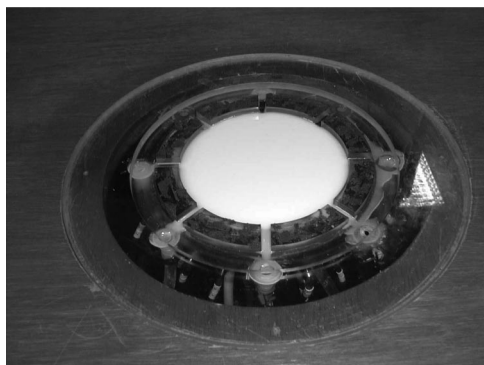


Fig. 2. Fluid-filled cup viewed from above.

fluid-filled cup and filled with fluid with the same optical properties as that in the cup to a height of 50 mm above the cup. The latex base of the cylinder is assumed to be sufficiently thin to have a negligible influence on the data.

C. Patient Scans

Suitable patients were recruited from among women attending appointments with breast surgeons. In most cases, a discrete lump had already been confirmed by conventional imaging (mammography or ultrasound). The patients received an optical scan either directly after their appointment at the clinic or arrangements were made for them to be scanned a few days later. Each scan took 11 min (using an illumination of 10 s per source). Scans were made of the diseased breast and, whenever possible, the healthy breast for comparison. Data were recorded simultaneously at both source wavelengths.

Thirty-eight patients, aged between 22 and 80 (mean 41 ± 15 yr old) with a variety of breast diseases were scanned: 19 women had one or more malignant lesions, 3 had cysts or galactoceals; 1 suffered from mastalgia, 1 had a leaking breast implant, 1 had a benign phyllodes, 1 had a malignant lesion in one breast and a fibroadenoma in the other, 1 had fibrocystic changes, and 11 had fibroadenomas.

D. Image Reconstruction

Three-dimensional images were generated from the data using the time-resolved optical absorption and scatter tomography (TOAST) reconstruction package developed at UCL [35]. TOAST employs the finite-element method (FEM) to model the propagation of light through tissue using the diffusion approximation to the radiative transfer equation. TOAST produces 3D images of scatter and absorption coefficients. Image reconstruction involves iteratively adjusting the optical properties assigned to the FEM mesh to minimize the difference between the data types predicted by the model and the data. The model starting values are the measured absorption and scatter coefficients of the coupling fluid. A hemispherical finite element mesh with the 50 mm cylindrical extension (to simulate the cup with the chest wall extension) with 46,415 tetrahedral elements and 67,537 nodes was generated using NETGEN software [36]. The mesh is assigned a greater density at the positions of the source–detector bundles, where the rate of change of light intensity is greater. The image reconstruction was performed using a conjugate gradient solver and Robin boundary conditions. In all cases, the 10th iteration was analyzed as this was found to be the number beyond which no further improvement to the images was observed. Each iteration required 48 min on a 2.2 GHz Xeon processor and used approximately 800 MB of RAM.

E. Derivation of Blood Volume and Oxygen Saturation

We assume that the optical absorption represented in the absorption images is due to three components: oxyhemoglobin (HbO_2), deoxyhemoglobin (Hb), and a

“background” component with the same absorption coefficient at both wavelengths (780 and 815 nm), assumed to be due to lipid and water. A background value of 70% of the absorption averaged over the image was selected, based on estimates of tissue optical properties published elsewhere [37]. However, we also tested the influence of the assumed size of the background by selecting a broad range of values between 55% and 85% of average absorption. The values of oxygen saturation varied by ~10%, while the blood volume varied by ~2%. The coefficient of variance for an individual image was greater than this, indicating that the absolute properties are not sensitive to changes in background.

The combination of data at two wavelengths and a knowledge of the appropriate extinction coefficients can be used to derive the regional blood volume (rBV) and the regional tissue oxygen saturation (rStO₂) as given below:

$$rStO_2 = \frac{[HbO_2]}{[HbO_2] + [Hb]}, \quad (1)$$

$$rBV = \frac{\text{volume of whole blood in tissue}}{\text{total tissue volume}}, \quad (2)$$

where [HbO₂] and [Hb] are the concentrations of oxyhemoglobin and deoxyhemoglobin, respectively. The normal range of values for hemoglobin concentration in blood [Hb_b] in the healthy adult female is 12.2–15.0 g/dl (1.9–2.3 mM), and a typical value of 14 g/dl (2 mM) is assumed here [38]. The regional blood volume (%) can be converted to an absolute unit of tissue hemoglobin (μmol of blood in 1000 cm³) assuming a hemoglobin concentration of 2 mM as given below:

$$rBV = \frac{[HbO_2] + [Hb]}{[Hb_b]} \times 100. \quad (3)$$

3. Results

The 38 patient studies produced 42 scans of pathologies (21 malignant and 21 benign) and 27 scans of healthy breasts. Some women had abnormalities in both breasts, but due to patient time constraints not all healthy breasts were scanned. Of all breast scans, a total of 58 images were obtained: 35 from pathological conditions and 23 of healthy breasts. A small number of scans failed to produce data sufficient to reconstruct an image, due to temporary instability in the system electronics or hardware malfunction.

Images typical of common types of lesion are shown, and the results obtained on the full cohort are discussed. Images representing scatter coefficient, blood volume, and oxygen saturation are shown. For each reconstructed 3D image, a single transverse slice across the breast-containing cup, at the level of the lesion, is displayed. Each scatter image obtained at 780 nm was qualitatively indistinguishable from the corresponding scatter image obtained at 815 nm

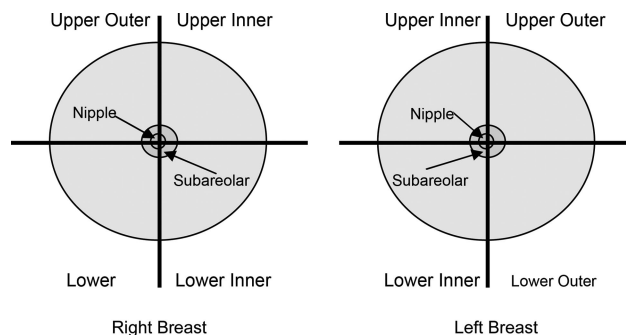


Fig. 3. Quadrants of the breast used to identify lesion locations.

and, in each case, only the scatter image at 780 nm is shown. The blood volume and blood oxygen saturation images are derived from the 10th iteration of the absorption images. The orientation of either breast in the cup is illustrated in Fig. 3. However, it is important to remember that the displayed images are of the entire cup. The breast often does not fill the cup, and the center of the cup does not necessarily correspond to the center of the breast. Where left and right breast images are shown together, a common color scale is employed.

A. Malignancy

Nineteen women with some form of malignancy in one or both breasts were scanned, with ages in the range of 26 to 56 yr (mean 48 ± 13 yr). The malignant conditions included carcinomas, a malignant phyllodes, and an intracystic carcinoma. The first three patients were scanned using only one wavelength, due to technical difficulties; therefore only absorption and scatter images at 780 nm were obtained, and it was not possible to derive the blood volume and blood oxygen saturation images. These first optical images are presented in Figs. 4(a)–4(c). The images shown are coronal slices of the 3D image of the breast through the region of the lesion with maximum contrast.

Figure 4(a) is of a 53 yr old woman with a large carcinoma behind the nipple of her left breast. Breast MRI demonstrated a 4.3 cm × 5.1 cm lobulated mass. The left breast only was scanned due to discomfort of the patient as a result of a bad back. The absorption image shows a region of increased absorption in the center of the image consistent with the known position of the lesion. The scatter image shows a corresponding region of increased scatter. This increase in scatter may be due to physiological changes in the cancerous cells or due to parameter cross talk, i.e., insufficient separation between the absorption and scatter parameters (as previously observed in optical images of the breast) [18,33].

Figure 4(b) shows the optical images from a 52 yr old woman with bilateral breast cancer. MRI images had revealed a distortion in the right breast, increased stroma in the right-upper and lower-outer quadrants of the breast, and a malignant mass in the left-upper-outer quadrant of the left breast. An in-

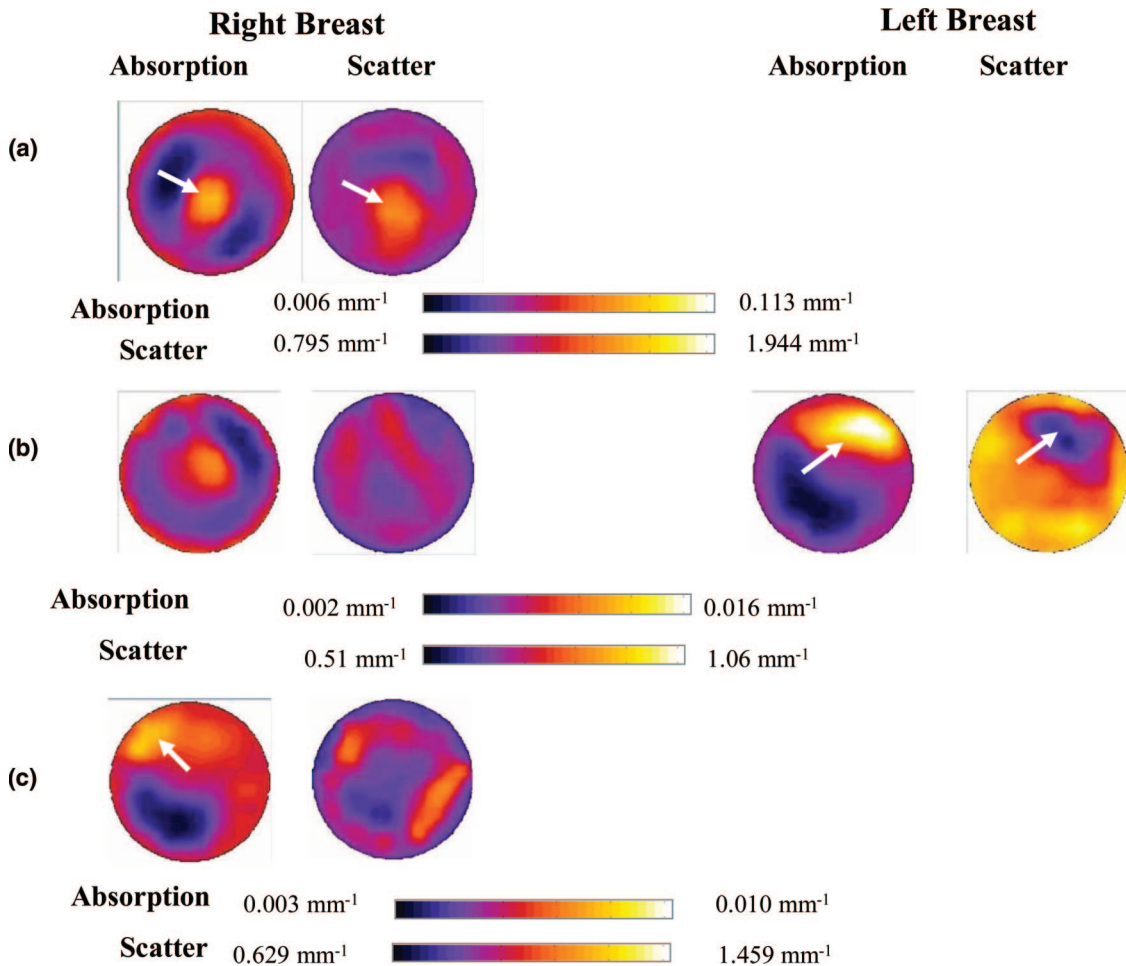


Fig. 4. (a) Absorption and scatter images from a 53 yr old woman with a large cancer in her left breast behind the nipple. (b) Absorption and scatter images of a 52 yr old woman with breast cancer. MRI showed a distortion in the right breast and increased stroma in the right-upper and lower-outer quadrants of the breast. In the left breast there is a malignant mass in the left-upper-outer quadrant. (c) Absorption and scatter images from a 36 yr old woman with a cancerous lesion in the upper-outer quadrant of her right breast.

creased region of absorption and decreased scatter can be seen in the images of the left breast in the upper-outer quadrant. No obvious lesions are seen in the right breast.

Figure 4(c) shows the optical images from a 36 yr old woman diagnosed with breast cancer in the upper-outer quadrant of her right breast. A MRI image indicated that the lesion measured 5.3 cm × 3.3 cm × 5.3 cm. Only the right breast was scanned, due to insufficient time before the patient had to return to the clinic.

All subsequent patients were scanned using both wavelengths, allowing us to derive oxygen saturation and blood volume maps. The images in Fig. 5(a) are from a 55 yr old woman with a 13 mm diameter intracystic carcinoma in the upper-outer quadrant of her right breast, in line with and 3 cm posterior to the nipple. The MRI showed poor enhancement in the center, indicating either calcifications or bleeding following aspiration or biopsy. Her left breast showed areas of enhancement in the lower-inner quadrant of the breast. Both breasts were scanned optically. The optical images of the diseased breast show a region of

increased scatter and decreased blood oxygen saturation in the region of the lesion that is not seen in the contralateral breast. The images are displayed on the same scale.

Figure 5(b) displays images from a 45 yr old woman with a carcinoma in the lower-inner side of her left breast. In the x-ray mammogram, there was an ill-defined 15 mm diameter mass in the left breast and the right breast was normal. Ultrasound demonstrated a 22 mm × 17 mm × 17 mm mass with vascularization. There were also two prominent lymph nodes in the upper-outer quadrant of the left breast. The optical images show an area of increased blood volume in the lower-inner quadrant of her left breast that is not seen in the right breast.

Of the 18 scans of malignancies that resulted in images, one case of ductal carcinoma *in situ* showed no changes in optical properties. Of the remaining 17, all show an increase in absorption, and all but one show an increase in blood volume. This correlates with what we know about angiogenesis occurring in the tumor. Eight of the tumors show a decrease in oxygen saturation in the region of the lesion, while

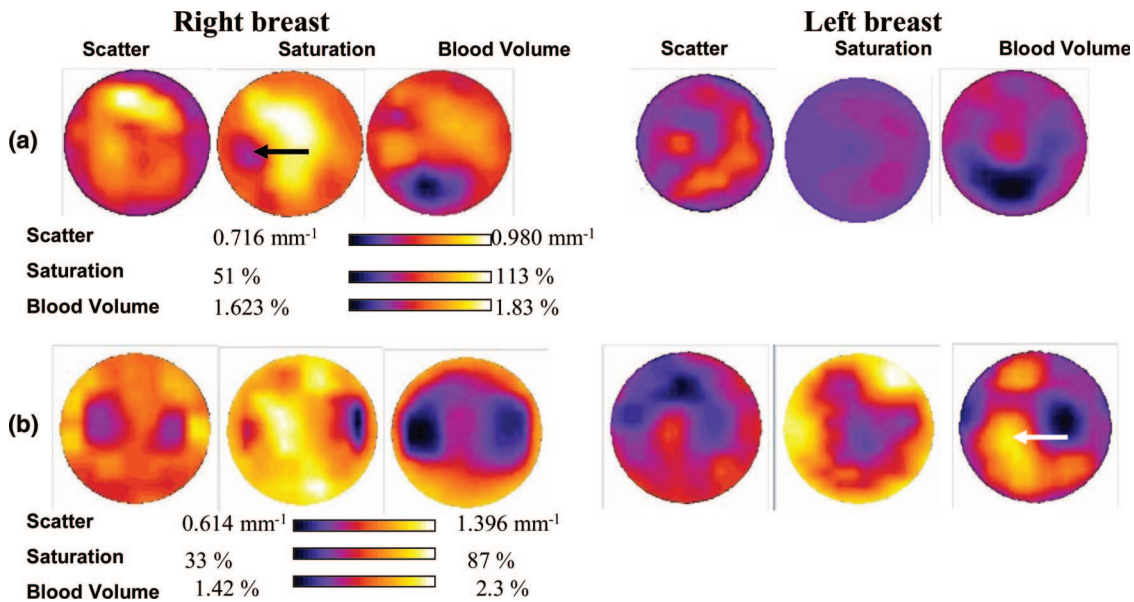


Fig. 5. (a) Scatter, blood volume, and blood oxygen saturation images from a 55 yr old woman with a 13 mm diameter intracystic carcinoma in the upper-outer quadrant of her right breast, in line with and 3 cm posterior to the nipple. (b) Scatter, blood volume, and blood oxygen saturation images from a 45 yr old woman with a carcinoma in the lower-inner side of her left breast.

the others show no change. Two of the tumors show no change in scatter, ten show an increase, and five show a decrease.

B. Fibroadenoma

Fibroadenomas are benign breast lumps with low vascularization and a distinctive histological appearance. They are most commonly seen in younger women and are usually assessed using mammography or ultrasound. They are sometimes identified as suspicious on mammograms, leading to unnecessary biopsies. Our previous study using the fixed ring of sources and detectors observed fibroadenomas in six patients with varied levels of contrast [18], largely consistent with another optical imaging study suggesting that fibroadenomas display no unique optical characteristics [17]. Twelve women diagnosed with fibroadenomas, with ages between 22 and 48 yr (mean 26 ± 6 yr), have so far been scanned using the liquid-coupled interface at UCL.

Figure 6(a) shows optical images from a 29 yr old, with a fibroadenoma in the lower-inner quadrant of her right breast. The ultrasound demonstrated a $8 \text{ mm} \times 11 \text{ mm} \times 5 \text{ mm}$ discrete mass. Both breasts were optically scanned. A region of increased blood volume and decreased oxygen saturation is seen in the images of the right breast.

The optical images in Fig. 6(b) are from a 48 yr old woman with a fibroadenoma reported to be in the upper-outer quadrant of her right breast. The fibroadenoma measured $11 \text{ mm} \times 5 \text{ mm} \times 7 \text{ mm}$ in size on the ultrasound and was positioned 3 cm from the nipple. The optical images show a region of decreased scatter at the expected location of the lesion and slightly increased blood oxygen saturation and blood volume.

Twelve women with fibroadenomas were scanned, resulting in 11 usable images. Of these images, four showed no obvious change in optical properties in the region of the lesion. Of the remaining seven, all showed an increase in absorption and blood volume. One showed an increase in scatter, while the other six showed a decrease. One showed an increase in oxygen saturation, while six showed a decrease.

C. Cysts

Cysts are fluid-filled sacs that develop within the breast tissue and are generally easily diagnosed upon ultrasound examination. The fluid in most cysts is optically clear, though sometimes there may be blood products present. Consequently cysts are commonly revealed in optical images as regions of very low scatter [20,33]. Three women aged between 27 to 57 yr (mean 40 ± 15 yr) were optically scanned. One of these women had cysts in both breasts, while another patient had three partially aspirated galactocele in the same breast, which are milk-filled cysts that develop in women who are breast-feeding. The third patient had three cysts located very close to each other in her left breast.

The breast images of the patient with the three galactocele exhibited regions of low scatter and high absorption. While the low scatter was expected, the high absorption may be due to minor bleeding following the partial aspiration. Meanwhile optical images of the women with three close cysts in her left breast [Fig. 6(c)] show regions of very low oxygen saturation and blood volume in the region of the group of cysts but no associated decrease in scatter. No similar features are seen in the contralateral breast. Unfortunately, data recorded on the third woman with cysts did not yield usable images.

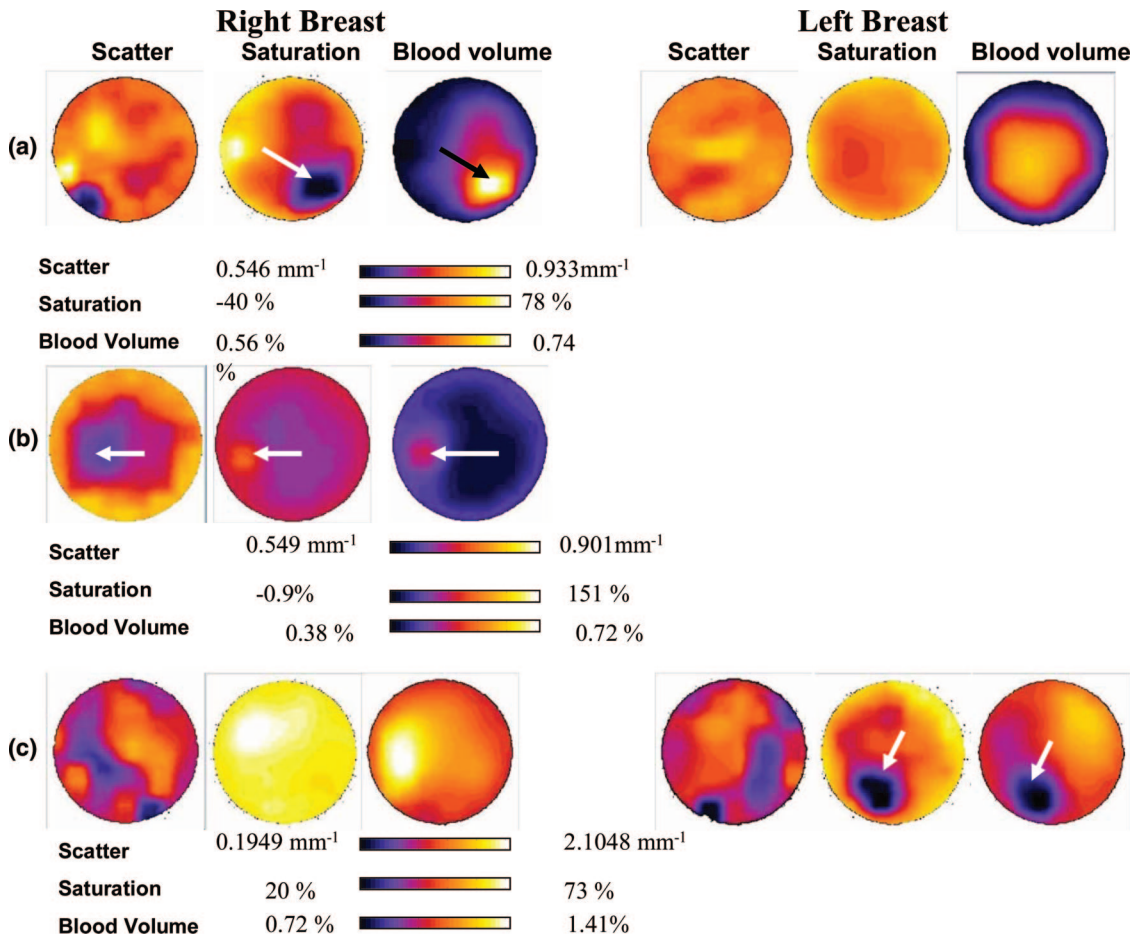


Fig. 6. (a) Images of a 48 yr old woman with an 11 mm × 5 mm × 7 mm fibroadenoma in the upper-outer quadrant of her right breast. (b) Images of a 29 yr old with a fibroadenoma in the lower-inner quadrant of her right breast. The ultrasound revealed a lump of 8 mm × 11 mm × 5 mm. (c) Images of a 27 yr old woman with three cysts in her left breast. The cyst diameters obtained from ultrasound were 29, 15, and 9 mm.

D. Other Benign Conditions

Four women with other benign conditions, aged between 30 and 44 yr (mean age 35 ± 6 yr), also took part in the study. One woman had a diagnosis of fibrocystic change (a condition that includes a range of changes within the breast involving both the glandular and stromal tissues). One of the women scanned had a leaking breast implant, one suffered from bilateral mastalgia, and one had a benign phyllodes tumor. Scans of the patients with the leaking implant and the benign phyllodes tumors did not yield data of sufficient quality from which to reconstruct images. No obvious lesions or changes in optical parameters were seen in the optical images from the patient with mastalgia, which is consistent with previously reported images [18]. The optical images from the patient with fibrocystic changes showed an increase in scatter in the expected region of the breast.

4. Discussion

In common with previous optical tomography studies, our initial results with the liquid-coupled system described above demonstrate good sensitivity to a broad

range of lesions; at least one of the optical images (scatter, blood volume, or blood oxygenation) usually shows some evidence of a prediagnosed lesion, unless it is very close to the chest wall, where the optical sampling is still relatively sparse. The good sensitivity is underlined by the results of the image classification shown in Table 1. Each set of breast images has been assessed using a quantitative scoring method proposed by Grosenick *et al.* [39] and Taroni *et al.* [17]. The scoring system is given in the footnote of the table. Scores vary between 0—which is assigned when the lesion produces no observable feature in any of the images, and 5—for an image where the dominant feature is due to the known lesion. An X means that a scan was performed but an image was not obtained due to an error occurring in the data collection or in the calibration measurement, which renders the data unusable. N/A means not applicable, when a discrete change in optical properties is not expected, such as in cases of mastalgia.

The optical images of breast cancer revealed a significant increase in absorption and regional blood volume in most cases, presumably as a result of tumor hypervascularization. Low blood oxygen saturation is

Table 1. Scoring System^a

Condition	Number of Cases and Scans Performed	Number of Images Obtained	Scores	Average Score
Carcinomas	21 (21)	18	5, 5, 0, 3, 5, 5, X, X, 4, 4, 4, X, 3, 5, 4, 5, 4, 5, 5, 5, 4	4.167
Cysts	4 (4)	2	5, 4, X, X	4.5
Fibroadenoma	12 (12)	11	5, 1, 4, 5, X, 4, 0, 0, 4, 3, 3, 5	3.09
Mastalgia	2 (2)	2	N/A	N/A
Other benign conditions	3 (3)	2	4, 3, X	3.5
Normal breast	34 (27)	23	N/A	N/A
Total	76 (69)	58		4.02

^a5, contrast of lesion dominates; 4, contrast comparable to other inhomogeneities; 3, contrast inferior to other inhomogeneities but still clearly identifiable; 2, weak contrast; 1, hardly perceivable inhomogeneity, only detected if position is known; 0, not visible; X, image not obtained.

also often observed at the location of the lesion, as is a decrease in scatter. However, the latter may be due to parameter cross talk (i.e., a change in one coefficient causing a small apparent change in the other). Cross talk was observed with previous phantom studies, described by Yates *et al.* [34]. In the case of the patient with an intracystic carcinoma, there is a decrease in blood oxygen saturation, increased scatter, and no evidence of increased blood volume [Fig. 5(a)]. Intracystic carcinomas are a rare form of breast cancer and do not behave like normal tumors. They are a form of papillary carcinoma, are slow growing, and are of low density [40]. Their slow growth may suggest that they do not develop the vasculature commonly associated with tumors.

Fibroadenomas have a normal vasculature, so little change in blood volume is expected. Only half of the fibroadenomas we scanned revealed any optical contrast in the region of the lesion relative to the surrounding tissue and/or the contralateral breast, which is consistent with results of other researchers [17]. All fibroadenomas that exhibited contrast indicated an increased blood volume, and all but one suggested a decrease in oxygen saturation. A study of *ex vivo* tissue properties has predicted a possible increase in absorption and low scatter for fibroadenomas [8].

Cysts are typically low-scattering regions, so a decrease in blood volume and oxygen saturation in the region of cysts, as well as a decrease in scatter, is expected and is commonly observed. However, the scans performed on patients with cysts did not produce images that conformed exactly with expectation. Three galactoceleas were exhibited as regions of low scatter and high absorption, probably due to aspiration-induced bleeding, while the cysts in another patient were revealed only as regions of low blood volume and oxygen saturation, with no evidence of low scatter. However, the scatter images for this 27 yr old subject exhibited a very high degree of heterogeneity in both breasts, which is commonly observed for younger women.

The observed maximum percent blood volume was 2.4% for tumors and 1.3% for benign lesions. These

values are equivalent to total hemoglobin [Hb_t] of 48 and 27 μM , respectively (assuming 2 mM hemoglobin concentration). Background values of $\sim 0.7\%$ – 1.5% are seen in both healthy and diseased breasts (13–30 μM). Cysts show a decrease in blood volume compared with the background tissue.

Because calculations include areas occupied by the coupling fluid, the blood oxygen saturation values displayed in the 3D images range from -0.7% to over 100%. However, when examining the regions occupied by the breast alone, the oxygen saturation values are within $56\% \pm 20\%$. Whereas blood volume depends on total absorption, determination of oxygen saturation requires more subtle spectroscopic changes. Other researchers have found bulk healthy tissue oxygen saturation values of $68\% \pm 8\%$ [41], $74\% \pm 9\%$ [23], and 67% – 70% [24].

A successful medical diagnostic technique usually requires more than just good sensitivity; it is necessary to distinguish between one type of pathology and another and between benign and malignant lesions, in particular. So far, our study has been exclusively retrospective and has intended to provide a preliminary indication of the typical appearance of a broad range of pathologies. The next important step is to establish the specificity of the imaging technique and determine if any optical signatures can be identified that are indicative of the type of lesion. Ultimately this requires a prospective study involving a sufficient number of patients so that a meaningful statistical analysis can be performed.

Better discrimination is being sought by improving both the spatial resolution and the quantitative accuracy of the images. Our efforts to achieve this are largely focused on introducing prior structural information into the image reconstruction and information on the boundary between the breast and the surrounding fluid in particular. One approach we are currently investigating involves deliberately using a coupling liquid with lower scatter and absorption in order to clearly identify the boundary in the images. This, combined with a knowledge of the breast volume derived from the displacement of fluid, enables

the reconstructed volume to be confined to that occupied by the breast.

Although improved quantitative accuracy is expected to help distinguish between lesions, a recent optical imaging study reported by Pogue *et al.* [19] has already identified a marked variation in the normal physiological parameters between patients and suggested that it may be necessary to examine the ratio of contrast between the lesion and the surrounding tissue rather than absolute values of optical parameters.

Finally, optical imaging of the breast offers a potentially powerful tool for monitoring long-term changes in the breast, such as the study of tissue recovering following surgery [33] or alterations during and after treatment with chemotherapy or radiotherapy. Since optical scanning is safe, repeated scans over a long period can be performed without the exposure risks associated with x-ray imaging.

The authors acknowledge the financial support of Cancer Research UK and the Engineering and Physical Sciences Research Council.

References

1. Office for National Statistics, *Mortality Statistics: Cause England and Wales 2004* (The Stationary Office, 2004).
2. L. Tabar, M.-F. Yen, B. Vitak, H.-H. Chen, R. A. Smith, and S. W. Duffy, "Mammography service screening and mortality in breast cancer patients: 20-year follow-up before and after introduction of screening," *Lancet* **361**, 1405–1410 (2003).
3. R. W. Blamey, A. R. M. Wilson, and J. Patnick, "Screening for breast cancer," *BMJ* **689**, 693 (2003).
4. M. D. Schnall, "Application of magnetic resonance imaging to early detection of breast cancer," *Breast Cancer Res.* **3**, 17–21 (2001).
5. D. D. Pavic, M. D. Koomen, C. D. Kuzmiak, and E. D. Pisano, "Ultrasound in the management of breast disease," *Curr. Womens Health Rep.* **3**, 156–164 (2003).
6. A. E. Cerussi, A. I. Berger, F. Bevilacqua, N. Shah, D. Jakubowski, J. Butler, R. F. Holcombe, and B. J. Tromberg, "Sources of absorption and scattering contrast for near infrared optical mammography," *Acad. Radiol.* **8**, 211–218 (2001).
7. S. B. Colak, M. B. van der Mark, G. W. Hooft, J. H. Hoogenraad, E. S. van der Linden, and F. A. Kuijpers, "Clinical optical tomography and NIR spectroscopy for breast cancer detection," *IEEE Quantum Electron.* **5**, 1143–1158 (1999).
8. V. G. Peters, D. R. Wyman, M. S. Patterson, and G. L. Frank, "Optical properties of normal and diseased human breast tissue in the visible and near infrared," *Phys. Med. Biol.* **35**, 1317–1334 (1990).
9. X. Cheng, J. Mao, R. Bush, D. B. Kopans, R. H. Moore, and M. Chorlton, "Breast cancer detection by mapping hemoglobin concentration and oxygen saturation," *Appl. Opt.* **42**, 6412–6421 (2003).
10. S. Jiang, B. W. Pogue, T. O. McBride, and K. D. Paulsen, "Quantitative analysis of near-infrared tomography: sensitivity to the tissue-simulating precalibration phantom," *J. Biomed. Opt.* **8**, 308–315 (2003).
11. A. Li, E. L. Miller, M. Kilmer, T. J. Brukilacchio, T. Chaves, J. J. Stott, Q. Zhang, T. Wu, M. Chorlton, R. H. Moore, D. B. Kopans, and D. A. Boas, "Tomographic optical breast imaging guided by three-dimensional mammography," *Appl. Opt.* **42**, 5181–5190 (2003).
12. C. H. Schmitz, D. P. Klemer, R. Hardin, M. S. Katz, Y. Pei, H. L. Graber, M. B. Levin, R. D. Levina, N. A. Franco, W. B. Solomon, and R. L. Barbour, "Design and implementation of dynamic near-infrared optical tomographic imaging instrumentation for simultaneous dual-breast measurements," *Appl. Opt.* **44**, 2140–2152 (2005).
13. Y. Young, M. Shnall, S. Zhao, S. Orel, C. Xie, S. Nioka, B. Chance, and A. Solin, "Optical imaging of breast tumour by means of continuous waves," *Adv. Exp. Med. Biol.* **441**, 227–232 (1997).
14. J. P. Culver, R. Choe, M. J. Holboke, L. Zubkov, T. Durduran, A. Slemple, V. Ntziachristos, B. Chance, and A. G. Yodh, "Three-dimensional diffuse optical tomography in the parallel plane transmission geometry: evaluation of a hybrid frequency domain/continuous wave clinical system for breast imaging," *Med. Phys.* **30**, 235–247 (2003).
15. B. W. Pogue, M. Testorf, T. McBride, U. Osterberg, and K. Paulsen, "Instrumentation and design of a frequency-domain diffuse optical tomography imager for breast cancer detection," *Opt. Express* **1**, 391–403 (1997).
16. D. Grosenick, H. Wabnitz, K. T. Moesta, J. Mucke, M. Moller, C. Stroszczynski, J. Stobel, B. Wassermann, P. M. Schlag, and H. Rinneberg, "Concentration and oxygen saturation of hemoglobin of 50 breast tumours determined by time-domain optical mammography," *Phys. Med. Biol.* **49**, 1165–1181 (2004).
17. P. Taroni, G. Danesini, A. Torricelli, A. Pifferi, L. Spinelli, and R. Cubeddu, "Clinical trial of time-resolved scanning optical mammography at 4 wavelengths between 683 and 975 nm," *J. Biomed. Opt.* **9**, 464–473 (2004).
18. T. D. Yates, J. C. Hebden, A. P. Gibson, N. L. Everdell, S. R. Arridge, and M. Douek, "Optical tomography of the breast using a multi-channel time-resolved imager," *Phys. Med. Biol.* **50**, 2503–2517 (2005).
19. B. W. Pogue, S. Jiang, H. Dehghani, C. Kogel, S. Soho, S. Srinivasan, X. Song, T. D. Tosteson, S. P. Poplack, and K. D. Paulsen, "Characterization of hemoglobin, water and NIR scattering in breast tissue: analysis of intersubject variability and menstrual cycle changes," *J. Biomed. Opt.* **9**, 541–552 (2004).
20. D. Grosenick, K. T. Moesta, M. Möller, J. Mucke, H. Wabnitz, B. Gabauer, C. Stroszczynski, B. Wassermann, P. M. Schlag, and H. Rinneberg, "Time-domain scanning optical mammography: I. Recording and assessment of mammograms of 154 patients," *Phys. Med. Biol.* **50**, 2429–2449 (2005).
21. D. Grosenick, H. Wabnitz, K. T. Moesta, J. Mucke, P. M. Schlag, and H. Rinneberg, "Time-domain scanning optical mammography: II. Optical properties and tissue parameters of 87 carcinomas," *Phys. Med. Biol.* **50**, 2451–2468 (2005).
22. P. Taroni, A. Torricelli, L. Spinelli, A. Pifferi, F. Arpaia, G. Danesini, and R. Cubeddu, "Time-resolved optical mammography between 637 and 985 nm: clinical study on the detection and identification of breast lesions," *Phys. Med. Biol.* **50**, 2469–2488 (2005).
23. L. Spinelli, A. Torricelli, A. Pifferi, P. Taroni, G. Danesini, and R. Cubeddu, "Characterization of female breast lesions from multi-wavelength time-resolved optical mammography," *Phys. Med. Biol.* **50**, 2489–2502 (2005).
24. T. O. McBride, B. W. Pogue, E. D. Gerety, S. B. Poplack, U. L. Osterberg, and K. D. Paulsen, "Spectroscopic diffuse optical tomography for the quantitative assessment of hemoglobin concentration and oxygen saturation in breast tissue," *Appl. Opt.* **38**, 5480–5490 (1999).
25. H. Dehghani, B. W. Pogue, S. P. Poplack, and K. D. Paulsen, "Multiwavelength three-dimensional near-infrared tomography of the breast: initial simulation, phantom and clinical results," *Appl. Opt.* **42**, 135–145 (2003).
26. B. W. Pogue, S. Jiang, X. Song, S. Srinivasan, H. Dehghani, K. D. Paulsen, T. D. Tosteson, C. Kogel, S. Soho, and S. P. Poplack, "Near-infrared scattering spectrum differences between benign and malignant breast tumours measured in vivo

- with diffuse tomography,” in *OSA Biomedical Topical Meeting* (2004).
27. R. Wiener, R. Choe, A. Corlu, K. Lee, S. M. Crinivas, J. R. Saffer, R. Freifelder, J. S. Karp, A. G. Yodh, and S. D. Konecky, “Diffuse optical tomography and positron emission tomography of human breast,” in *Biomedical Optics Topical Meeting* (2006).
 28. R. Choe, A. Corlu, K. Lee, T. Durduran, S. D. Konecky, M. Grosicka-Koptyra, S. R. Arridge, B. J. Czernieki, D. L. Fraker, A. DeMichele, B. Chance, M. A. Rosen, and A. G. Yodh, “Diffuse optical tomography of breast cancer during neoadjuvant chemotherapy: a case study with comparison to MRI,” *Med. Phys.* **32**, 1128–1139 (2005).
 29. X. Intes, J. Ripoll, Y. Chen, S. Nioka, A. G. Yodh, and B. Chance, “In vivo continuous-wave optical breast imaging enhanced with Indocyanine Green,” *Med. Phys.* **30**, 1039–1047 (2003).
 30. O. Zhang, T. I. Brukilacchio, A. Li, J. J. Scott, T. Chaves, E. Hillman, T. Wu, M. Chorlton, E. Rafferty, R. H. Moore, D. B. Kopans, and D. A. Boas, “Coregistered tomographic x-ray and optical breast imaging: initial results,” *J. Biomed. Opt.* **10**, 024033 (2005).
 31. B. J. Tromberg, A. Cerussi, N. Shah, M. Compton, A. Durkin, D. Hsiang, J. Butler, and R. Mehta, “Diffuse optics in breast cancer: detecting tumours in pre-menopausal women and monitoring neoadjuvant chemotherapy,” *Breast Cancer Res.* **7**, 279–285 (2005).
 32. F. E. W. Schmidt, M. E. Fry, E. M. C. Hillman, J. C. Hebden, and D. T. Delpy, “A 32-channel time-resolved instrument for medical optical tomography,” *Rev. Sci. Instrum.* **71**, 256–265 (1998).
 33. J. C. Hebden, T. D. Yates, A. Gibson, N. Everdell, S. R. Arridge, D. W. Chicken, M. Douek, and M. R. S. Keshtgar, “Monitoring recovery after laser surgery of the breast with optical tomography: a case study,” *Appl. Opt.* **44**, 1898–1904 (2005).
 34. T. D. Yates, J. C. Hebden, A. P. Gibson, L. Enfield, N. L. Everdell, S. R. Arridge, and D. T. Delpy, “Time-resolved optical mammography using a liquid coupled interface,” *J. Biomed. Opt.* **10**, 054011 (2005).
 35. S. R. Arridge, J. C. Hebden, M. Schweiger, F. E. W. Schmidt, M. E. Fry, E. M. C. Hillman, H. Dehghani, and D. T. Delpy, “A method for 3D time-resolved optical tomography,” *Int. J. Imaging Syst. Technol.* **11**, 2–11 (2000).
 36. J. Schöberl, “NETGEN—an advancing front 2d/3D-mesh generator based on abstract rules,” *Comput. Vision Sci.* **1**, 41–52 (1997).
 37. S. J. Matcher, M. Cope, and D. T. Delpy, “Use of the water absorption spectrum to quantify tissue chromophore concentration changes in near-infrared spectroscopy,” *Phys. Med. Biol.* **38**, 177–196 (1993).
 38. E. M. C. Hillman, “Experimental and theoretical investigations of near-infrared tomographic imaging methods and clinical applications,” Ph.D. thesis (University of London, 2002).
 39. D. Grosenick, K. T. Moesta, H. Wabnitz, J. Mücke, C. Stroszczyński, R. Macdonald, P. M. Schlag, and H. Rinneberg, “Time-domain optical mammography: initial clinical results on detection and characterization of breast tumours,” *Appl. Opt.* **42**, 3170–3186 (2003).
 40. M. A. Peters, D. R. Voegeli, and K. A. Scanlan, *Breast Imaging* (Churchill-Livingstone, 1989).
 41. S. Fantini, S. A. Walker, M. A. Franceschini, M. Kaschke, P. Schlag, and K. T. Moesta, “Assessment of the size, position and optical properties of breast tumors in vivo by noninvasive optical properties,” *Appl. Opt.* **37**, 1982–1989 (1998).